Available online at www.sciencedirect.com
ScienceDirect
Journal of the European Ceramic Society 30 (2010) 3363–3375
www.elsevier.com/locate/jeurceramsoc

Microstructure-mechanical-tribological property correlation of multistage spark plasma sintered tetragonal ZrO_2

K. Madhav Reddy [a], Amartya Mukhopadhyay [a,b], Bikramjit Basu [a,*]

[a] *Department of Materials Science and Engineering, Indian Institute of Technology, IIT Kanpur, India*
[b] *School of Engineering, Brown University, Providence, RI, USA*

Received 7 April 2010; received in revised form 24 July 2010; accepted 2 August 2010
Available online 24 August 2010

Abstract

We report here the development of dense yttria-stabilized t-ZrO_2 ceramics with more uniform and finer grain sizes and concomitantly better mechanical and tribological properties via multistage spark plasma sintering (SPS). The dense tetragonal ZrO_2 ceramics were obtained by adopting three different SPS heating cycles, designed on the basis of fundamental sintering theory. The suppression of grain growth to nanosize regime (∼100–150 nm), along with the development of more uniform grain size distribution was achieved with multistage sintering (MSS), as compared to normal single stage sintering (SSS). Finer microstructural scale, along with superior hardness also led to improved fretting wear resistance for the ZrO_2 samples processed via MSS. Based on the experimental results and analysis, a correlation has been established between the SPS processing schemes, microstructural development and mechanical as well as tribological properties of the tetragonal ZrO_2. The effectiveness of MSS to produce tetragonal ZrO_2 ceramics with better mechanical and tribological properties was confirmed at two different levels of yttria content (3 and 2 mol%).

Keywords: Spark Plasma Sintering; ZrO_2; Nanomaterial; Microstructure; Properties

1. Introduction

Spark plasma sintering has been in extensive use for the last few decades for fabricating materials on a laboratory scale.[1,2] It has been widely recognized now that this process enables powders to be sintered to full density at lower temperatures and shorter sintering time, compared to pressureless sintering processes.[3–5] Phenomenologically, SPS process involves heating of a porous powder compact, by means of DC pulse, which is applied through electrodes at the top and bottom punches of the graphite die. SPS is widely used for faster densification of ceramics, composites, intermetallics and functionally gradient materials.[6–9] Despite having specific advantages like rapid rate of heating and lower processing time, one of the major disadvantages of SPS process is massive sparking, which occurs during the rapid heating, expedites abnormal grain growth during sintering.[10] Another disadvantage is that uniform densification depends on size of the sample.[11,12] Although not reported extensively in the literature, SPS process can lead to non-uniformity in densification and concomitantly variation in material properties across the sample width/thickness.[13,14] These restrict wider industrial applications of the SPS process.

Among oxide ceramics, tetragonal zirconia polycrystals (TZP) has excellent combination of strength and toughness, wear resistance, high chemical and corrosion resistance, as well as biocompatibility. Such combination of properties makes ZrO_2 a strong candidate for various structural and biomedical applications. The commercial applications of ZrO_2-based materials include femoral ball heads, dental restoratives, extrusion dies, seal faces and milling media.[15]

With regard to the SPS process, densification of ZrO_2 and ZrO_2-based composites via normal single step sintering has been studied by many research groups.[10,16–19] Systematic studies have been carried out on the effect of the SPS parameters, i.e. temperature, time, heating rate and pressure on the mechanical properties. The experimental results suggest that full densification of ZrO_2 ceramics can be accomplished at lower sintering temperature (1200–1300 °C) and relatively shorter

* Corresponding author. Tel.: +91 512 2597771; fax: +91 512 2597505.
E-mail addresses: bikram@iitk.ac.in, basubikram@yahoo.com (B. Basu).

0955-2219/$ – see front matter © 2010 Elsevier Ltd. All rights reserved.
doi:10.1016/j.jeurceramsoc.2010.08.005

dwelling time (0–5 min) compared to the conventional pressureless sintering process.[20,21] Yoshimura et al.[22] also reported that strength and hardness vary with SPS temperature. The hardness and strength of nanocrystalline 3Y-ZrO_2 (3 mol% yttria-stabilized zirconia) ceramics have been reported to vary between 12–14 GPa and 500–1500 MPa, respectively.[23]

Few attempts have been made to improve the microstructure of sintered ceramics via two step sintering, using conventional pressureless sintering as well as SPS technique.[24,25] Such two step sintering process via pressureless sintering involves heating the samples to relatively high (sintering) temperatures for attaining intermediate densities, followed by reducing the temperature by ~150 °C and holding for longer time (20 h) for achieving near theoretical density, while minimizing grain growth.[26,27] The disappearance of closed pores, while restricting grain growth in case of ZrO_2, Al_2O_3 and Y_2O_3 ceramics were demonstrated using the above-mentioned two stage sintering process.[28,29]

In the above perspective, the present work reports the results of a set of exploratory SPS experiments, which involve single-stage, two-stage and multi-stage heating of ZrO_2 ceramics. The heating rate was maintained at ~200 °C/min till the final sintering temperature of 1250 °C was reached (single stage sintering or SSS). Holding at intermediate temperature of 980 °C (two stage sintering or TSS) and subsequently holding at 1100 °C (multistage sintering or MSS) were carried out before the final sintering temperature (of 1250 °C) was reached for the innovative SPS heating schemes. The heating rate was maintained at ~200 °C/min similar to the SSS. Initial set of experiments were carried out on commercially available 3 mol% yttria-stabilized ZrO_2 powders (T3-ZrO_2). Subsequently, similar set of SPS experiments was also conducted on powder mixtures of 3Y-ZrO_2 and yttria-free ZrO_2 powders (2:1 ratio) to give a net yttria-stabilizer content of 2 mol%. Use of different starting powders enabled us to assess the reproducibility and efficacy of the innovative MSS route for processing ZrO_2 ceramics with different stabilizer contents. The use of TM2-ZrO_2 powders, in addition to T3-ZrO_2, has also been made in the light of the fact that for ZrO_2 ceramics, the mechanical properties are sensitive to the yttria-stabilizer content.[15] Furthermore, earlier reports have shown that t-ZrO_2 ceramics developed from such mixed starting powders often possess superior mechanical properties, as compared to those developed from commercially available 3Y-TZP powders.[15] It will be explored if multistage sintering via SPS can enable one to obtain more uniform and finer microstructure development and concomitantly uniform and improved mechanical properties. Additionally, fretting wear tests were conducted on mixed ZrO_2 ceramic, sintered via single stage and multi stage sintering to study the effects of SPS sintering schemes and consequent microstructural development and mechanical properties on the tribological properties.

2. Experimental

2.1. Processing

The commercially available 3 mol% yttria co-precipitated ZrO_2 (Tosoh grade TZ-3Y) and yttria-free ZrO_2 (Tosoh grade TZ-0Y) powders were used in the present investigation. According to the powder supplier, the crystallite size of the ZrO_2 powder is ~27 nm. 3 mol% yttria and yttria-free ZrO_2 powders were taken in a ratio of 2:1 and ball milled for 24 h in the presence of wet media (toluene). The TZ-3Y powders alone were also ball milled under the same conditions. Samples processed from such powder mixtures containing overall 2 mol% yttria were designated as TM2-ZrO_2, while those processed from the TZ-3Y powders were designated as T3-ZrO_2. The dried milled powders were placed in cylindrical graphite dies with inner diameter 15 mm, and height 30 mm lined with graphite sheet, which were then placed inside the SPS chamber (Dr. Sinter, Model 515S, SPS syntax Inc., Japan). The die wall thickness was 8 mm. Sintering temperature was monitored by a pyrometer focused on the surface of the graphite die and sintering behavior was monitored by measuring change in the axial dimension of the compact body. After the final stage of holding at the sintering temperature, the power was turned off and the sample was allowed to cool down naturally in the vacuum chamber. For TSS and MSS, at each holding temperature, also at the final sintering temperature of 1250 °C, holding time of 5 min was maintained. On the basis of basic sintering theory, the different holding temperatures were selected (at $0.37T_m \sim 980$ °C and $0.4T_m \sim 1100$ °C). It is hypothesized that neck formation and elimination of continuous open pores would be the dominant mechanism at intermediate holding. The closer of residual pores can take place at the final sintering temperature ($0.45T_m \sim 1250$ °C). Such selection was made basically by following the piston displacements during a normal single stage sintering heating cycle. In the same way, intermediate holding temperatures were selected in our earlier report concerning MSS of Al_2O_3.[30] Uniaxial pressure of 30 MPa and a heating rate of ~200 °C/min were applied during the entire cycles for all the processing schemes. After sintering, the cylindrical discs of 15 mm diameter with a height of 3 mm were obtained.

2.2. Characterization

The sintered densities of the samples were measured using the Archimedes' principle. The X-ray diffraction (XRD) studies were performed using Cu Kα X-ray radiation (Rich-seifert, Germany, 200D) for determination of phase assemblage. Vickers microhardness tester was used for measuring hardness with an applied load of 100 g. Such a low load was selected to avoid any cracking from indent corners. The disc samples were cut into rectangular bars of $15 \times 3 \times 3\ mm^3$ in size. The vertical section (along pressure direction) was polished and Vickers indents were taken at every 3 mm distance along radial direction and at depths of 0.5, 1.5 and 2.5 mm distance along axial direction from surface. Such comprehensive hardness measurement can reveal non-uniformity in properties. The flexural strength of the ZrO_2 samples was tested in the 3-point bending mode using Instron 1195 Universal Testing Machine. For the strength measurements, the SPSed compacts were machined into bar shapes with desired dimensions ($15 \times 3 \times 3\ mm^3$). For the 3-point bend tests, a fixed span length of 12 mm and a constant loading speed of 0.1 mm/min were employed.

Table 1
Summary of research results illustrating the overall sinter density, grain size and flexural strength of SPS processed T3-ZrO_2 and TM2-ZrO_2.

Material	SPS process details	Overall sinter density (% ρ_{th})	Grain size (μm)	Flexural strength (3-point bending) (MPa)
T3-ZrO_2	Single stage sintering (SSS); 1250 °C, 5 min	98.5%	Sample edge: 0.27 ± 0.11 Sample centre: 0.15 ± 0.06	560.0 ± 168
T3-ZrO_2	Two stage sintering (TSS); 980 °C, 5 min; 1250 °C, 5 min	99.0%	Sample edge: 0.27 ± 0.11 Sample centre: 0.24 ± 0.09	585.0 ± 85
T3-ZrO_2	Multi stage sintering (MSS); 980 °C, 5 min; 1100 °C, 5 min; 1250 °C, 5 min	99.8%	Sample edge: 0.15 ± 0.05 Sample centre: 0.14 ± 0.04	746.5 ± 65
TM2-ZrO_2	Single Stage Sintering (SSS); 1250 °C, 5 min	98.9%	0.24 ± 0.07	625.0 ± 45.0
TM2-ZrO_2	Two Stage Sintering (TSS); 980 °C, 5 min; 1250 °C, 5 min	99.2%	–	1037.0 ± 62.5
TM2-ZrO_2	Multi Stage Sintering (MSS); 980 °C, 5 min; 1100 °C, 5 min; 1250 °C, 5 min	99.6%	0.09 ± 0.02	1350.0 ± 143.0

The ground and metallographically polished surfaces of T3-ZrO_2 were thermally etched for 10 min at a temperature of 200 °C lower than final sintering temperature. Subsequently, the etched surfaces were gold coated prior to Scanning Electron Microscopy (SEM) observation. The microstructural investigations of the TM2-ZrO_2 samples were performed by Transmission Electron Microscopy (TEM). The TEM observations were performed using a 200 kV Tecnai G^2 T-20 UTWIN microscope (FEI, Eindhoven, Netherlands), equipped with a high-angle annular dark field (HAADF) detector.

In order to assess any potential advantage of the different sintering cycles on the tribological properties, the friction and wear properties, as well as the underlying material removal mechanisms of TM2-ZrO_2 materials, were studied against widely used Al_2O_3, ZrO_2 and steel counter bodies. The fretting wear experiments were conducted at constant load (5 N) at an oscillating frequency of 5 Hz and 100 μm linear stroke for durations of 100,000 cycles. The wear scar profiles on each sample were obtained using a computer controlled Laser Surface Profilometer (Mahr-Perthometer PGK 120, Germany). The wear volumes were calculated by integrating the surface area of each 2-D profile (extracted from different locations on 3-D profile) over distance for TM2-ZrO_2 surfaces. From the estimated wear volumes, the specific wear rates [wear volume/(load × total fretted distance)] were calculated. In order to identify the dominant wear mechanisms, the worn surfaces were examined using SEM, equipped with Energy Dispersive X-ray Spectroscopy (EDS). Raman Spectrometer (WITec GmbH, Germany, alpha 300 series microscope), equipped with a furnace cooled charge coupled device (CCD) and argon ion laser with a wavelength of 514 nm, was used to study phase changes during the wear fretting wear tests. Raman spectra were recorded in the extended scan mode with acquisition time of 2–5 min.

3. Results

3.1. Densification behavior

Irrespective of the spark plasma sintering schedule, all the SPSed T3-ZrO_2 and TM2-ZrO_2 samples exhibited high overall sinter densities of 98–99.8% ρ_{th} (see Table 1). Careful observation revealed that MSS and TSS led to marginally higher overall sinter densities than SSS for both the types of ZrO_2 samples. The densification behavior during different SPS processing sequences was also assessed by monitoring time-dependent changes in the densification parameter (Ψ) (see Fig. 1), which is defined as;

$$\Psi = (\rho_t - \rho_i)/(\rho_{th} - \rho_i) \quad (1)$$

where ρ_t is the instantaneous density, ρ_i is the initial density, ρ_{th} is the theoretical density of the compact. A closer look at Fig. 1 revealed larger shrinkage between first and second holding, in comparison to that between second and final stage of holding. Also, noticeable increase in Ψ value was recorded at each holding stage, except during holding at final sintering temperature. For T3-ZrO_2 (Fig. 1a), during sintering via SSS, the Ψ value increased continuously from 600 °C to final sintering temperature 1250 °C till the sintered density reached ~98% ρ_{th}. On the other hand, the densification parameter slightly increased in TSS during the holding stage at temperature of 980 °C for 5 min. However, during rapid heating above temperature 980 °C, the Ψ value constantly increased up to 1250 °C, before the final stage

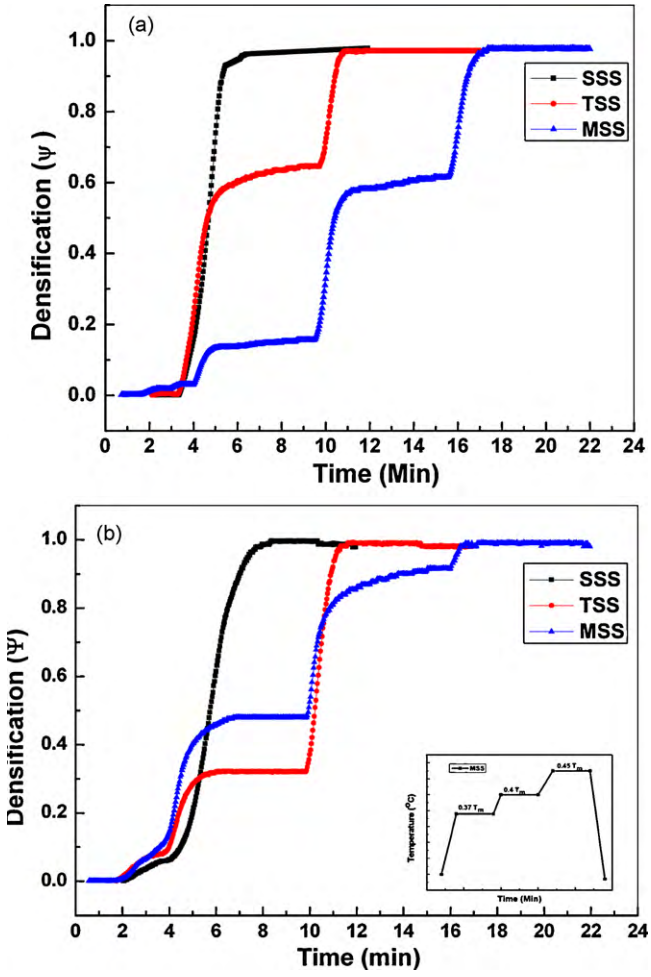

Fig. 1. Evolution of densification parameter; Ψ [=$(\rho_t - \rho_i)/(\rho_{th} - \rho_i)$]; as a function of heating time for (a) T3-ZrO_2 and (b) TM2-ZrO_2 during SPS processing via the three different sintering schedules—SSS, TSS and MSS.

of sintering was reached. In MSS, similar to that of TSS, Ψ values increased slightly during first and second holding stage, i.e. 980 °C and 1100 °C for 5 min at each temperature. Therefore, for T3-ZrO_2, marginally higher densification is recorded for MSS in comparison with SSS and TSS schedules. The densification behavior to reach final sinter density within such a close window can depend strongly on sintering schedule. Fig. 1b presents the densification behavior in terms of variation in the Ψ parameter with temperature for TM2-ZrO_2 ceramic. In case of SSS, the Ψ value increased monotonically from 600 to 1250 °C before the final sintering temperature was reached. In TSS, the Ψ value remained constant during the holding stage at 980 °C for 5 min. However, Ψ value increased constantly after the holding stage and the densification was nearly complete just before the final holding stage. In MSS, similar to TSS, the Ψ value remained constant during first holding stage. By contrast, at the second stage holding the Ψ value was observed to increase considerably (by ~0.1). A comparison of Fig. 1a and b reveals that the increase in Ψ value between two holding stages is by far more significant for TM2-ZrO_2 compared to that for T3-ZrO_2. We also believe that the first holding at $0.37T_m$ (T_m—melting point of ZrO_2) encourages the electrical discharge induced surface activation and ensures good particle-to-particle contact. This acts as a precursor to allow faster grain boundary diffusion during holding at second stage holding. In order to verify this, we carried out additional experiments to consolidate TM2-ZrO_2 powders to $0.37T_m$ (density ~68% ρ_{th}) and to $0.4T_m$ (density ~79% ρ_{th}) using single stage heating schedule. Similarly, the experiment was carried out for TSS, heating to a temperature $0.37T_m$ and soaking for 5 min, then further heating to a temperature of $0.4T_m$ and holding for 5 min; this resulted in slight increase in densification (81.5% ρ_{th}). Therefore, it should be clear that the third ramp of heating from 0.4 to $0.45T_m$ enhanced densification from ~81.5% ρ_{th} to 98.9–99.6% ρ_{th} respectively (see Fig. 1b).

Table 2
Sinter densities (gm/cm^3) measured for different sections cut along the radial direction, showing the variations in densification from centre to sample edges for the TM2-ZrO_2 and T3-ZrO_2 samples SPS processed following the different schemes (SSS, TSS and MSS).

Sectioned samples	TM2-SSS	TM2-TSS	TM2-MSS
Edge (E1)	6.028	6.068	6.06
Centre (C1)	5.85	5.637	6.065
Centre (C2)	5.51	5.82	6.03
Centre (C3)	5.79	5.998	–
Edge (E2)	6.05	6.01	6.10

Sectioned samples	T3-SSS	T3-TSS	T3-MSS
Edge (E1)	5.961	6.030	6.005
Centre (C1)	6.00	5.967	5.9829
Centre (C2)	5.857	–	5.9829
Edge (E2)	5.902	5.990	5.9758

In order to explore the effects of the SPS processing schemes (SSS, TSS and MSS) on the uniformity of the densification along the radial direction (edges to centre), the samples were accordingly cut into three/four sections and sintered densities were measured for each section (see Table 2). An important observation is the large variation in sintered density from the edges to the centre for both the TM2-ZrO_2 and T3-ZrO_2 ceramics after spark plasma sintering using SSS scheme. The densities were measured to be higher near the edges as compared to those near the centre. On the contrary, such variation was suppressed for the TSSed samples and was nearly non-existent for the MSSed samples. Hence, the present work has revealed for the first time that SPS processing via the MSS and TSS schemes lead to uniform densification along the radial direction, as opposed to the commonly used SSS scheme.

3.2. Microstructure development

XRD patterns (Fig. 2a and b) recorded from the polished surfaces of the as-sintered ZrO_2 samples revealed that only tetragonal ZrO_2 was present in all the samples, irrespective of the starting powder types (T3-ZrO_2 or TM2-ZrO_2) or the heating schedules (SSS, TSS or MSS). SEM images obtained from near the centre and the edge (along the radial direction) of polished and thermally etched T3-ZrO_2 compacts are presented in Figs. 3 and 4, respectively. Overall, nanosized grains, possessing equiaxed morphology, could be retained after SPS processing

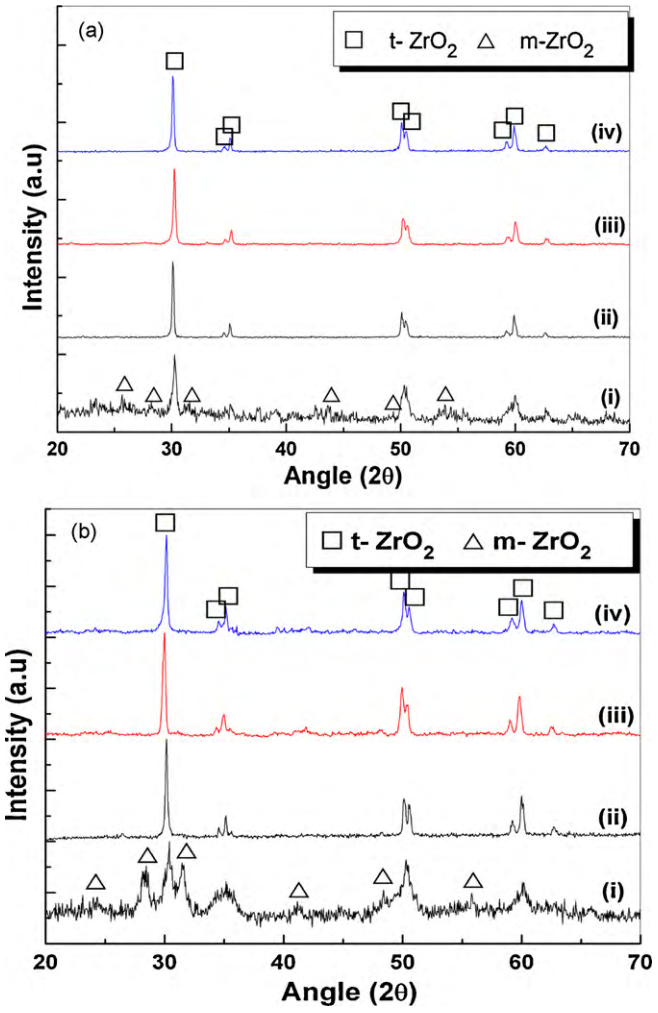

Fig. 2. XRD patterns recorded with (i) starting powders T3 and TM2, (ii) single stage sintered (SSS), (iii) two stage sintered, (iv) multi stage sintered (a) T3-ZrO_2 and (b) TM2-ZrO_2.

following all the three processing schemes. However, considerable differences between the average grain sizes and grain size distributions were noted for the samples sintered following the three different processing schemes (SSS, TSS and MSS). The grain sizes obtained with the different processing schemes were estimated using image analysis and the mean grain sizes, along with the standard deviations (as errors), are reported in Table 1. It can be observed that the ZrO_2, developed after MSS possessed the minimum average grain size (~150 nm). The influence of the three different SPS schedules (SSS, TSS and MSS) on the microstructure development can also be assessed from the differences in grain size distributions (GSD), which are shown as insets with the corresponding SEM micrographs in Figs. 3 and 4. In the case of SSS and TSS, the GSDs are more skewed type with long right hand side tail, indicating the presence of considerable number of grains, which were coarser than the mean grain size (see insets of Figs. 3 and 4a and b). On the contrary, for the sample developed after MSS, grain size distribution was found to be more uniform with the peak in GSD being recorded at around 100–200 nm (see inset of Figs. 3 and 4c). Comparisons of the SEM images obtained at different locations along

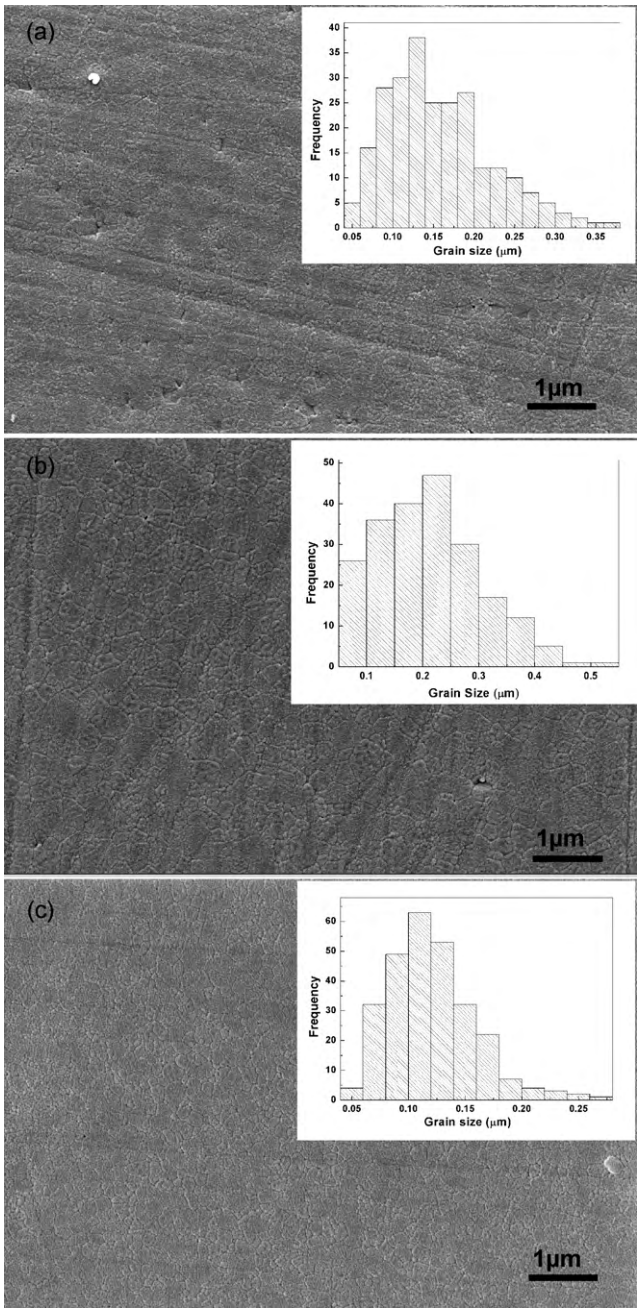

Fig. 3. SEM images obtained from the ground, polished and thermally etched surfaces near the sample cores of T3-ZrO_2 samples spark plasma sintered at 1250 °C via the three different routes (a) SSS; (b) TSS and (c) MSS. The grain size distributions are presented as insets of the corresponding images.

the radial directions reveal that while the mean grain sizes for the MSSed (average ~ 150 nm) and TSSed (average ~ 240 nm) samples show negligible variations with distance along the radial direction, the grains near the centre (Fig. 3a; average ~ 150 nm) are considerably smaller than those near the edge (Fig. 4a; average ~ 270 nm) in the case of SSS (see Figs. 3 and 4). More importantly, significant amount of porosity can be observed near the centre of the SSSed sample (Fig. 3a), while near the edge the sample appears to be fully dense. By contrast, no trace of residual porosity could be found for the MSSed sample, both near the edge (Fig. 4c) as well as near the centre (Fig. 3c).

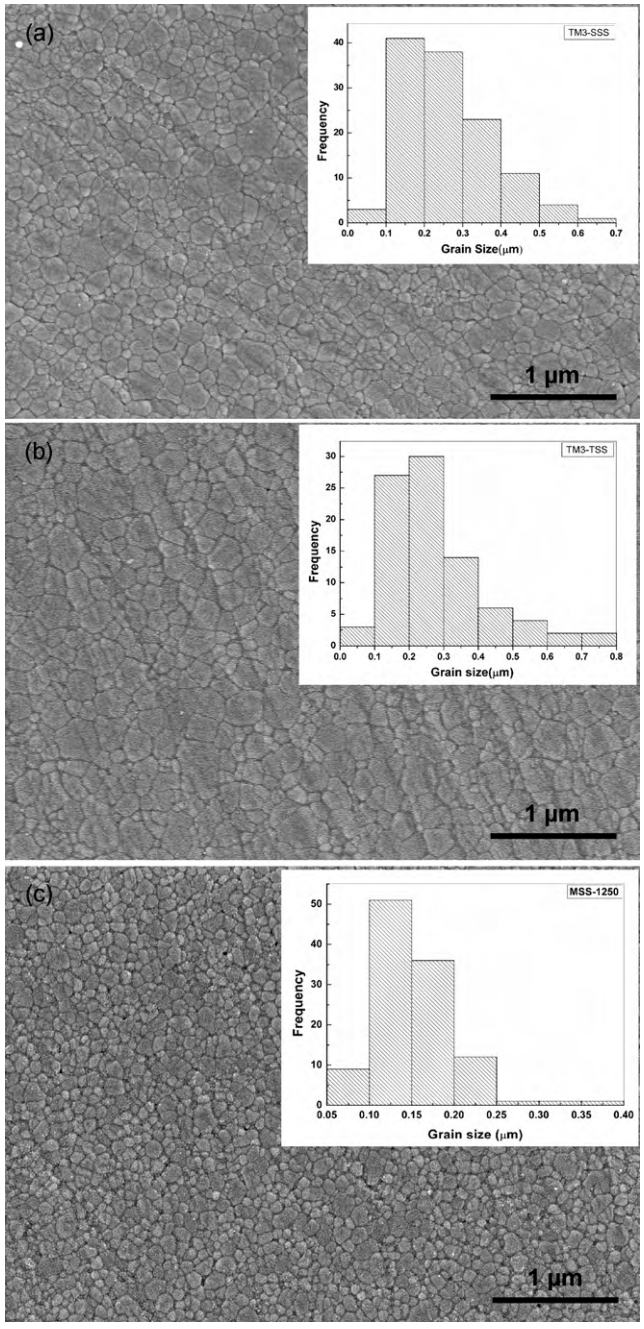

Fig. 4. SEM images obtained from the ground, polished and thermally etched surfaces near the sample edges of T3-ZrO_2 samples spark plasma sintered at 1250 °C via the three different routes (a) SSS; (b) TSS and (c) MSS. The grain size distributions are presented as insets of the corresponding images.

Such SEM observations further confirm the results obtained via Archimedes' method that differential densification occurred from the edge to the centre during SSS, while MSS helped prevent such density gradient (see Table 2 and Section 3.1).

Representative bright field TEM images obtained from the SSSed and MSSed TM2-ZrO_2 samples are presented in Fig. 5. The diffraction (ring) patterns obtained from the polycrystalline samples are presented as insets of the corresponding images. The diffraction patterns confirm that t-ZrO_2 phase was stabilized in the TM2-ZrO_2 samples sintered following both the processing

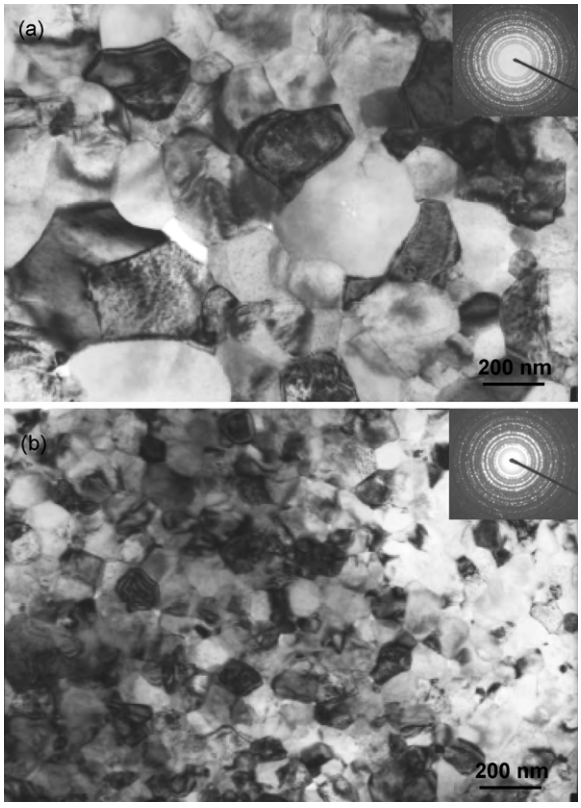

Fig. 5. Bright field TEM images of the TM2-ZrO_2 spark plasma sintered at 1250 °C via two different schedule (a) single stage sintering (SSS) and (b) multi stage sintering (MSS). The diffraction (ring) patterns obtained from the polycrystalline samples are presented as insets.

schemes. While extremely fine nanosized grains can be observed for the MSSed sample (average grain size: 90 nm), the SSSed sample showed relatively coarser grains (average grain size: 240 nm), which agreed with similar observations made for the T3-ZrO_2 samples. Also, similar to the T3-ZrO_2 samples, the grain size distribution plots revealed a considerably narrower grain size distribution (GSD from 60 to 130 nm) for the sample sintered via MSS as compared to SSS (GSD from 50 to 400 nm). Hence, the TEM observations also confirm that SPS processing via the innovative multistage sintering (MSS) scheme led to considerable suppression of the grain growth, resulting in the development of ZrO_2 nanoceramics as compared to the normal single stage sintering (SSS) scheme.

3.3. Mechanical properties

The microhardness was measured at different distances along the radial direction from one edge of the SPS processed ZrO_2 samples to the other. The variations in hardness with distance along the radial direction are presented in Fig. 6. Such measurements were made at three different depths of 0.5, 1.5 and 2.5 mm along the axial directions from the surface. The error bars in Fig. 6 indicate the spread in the hardness along the axial directions. It can be observed that for both the ZrO_2 samples (see Fig. 6a and b), SSS led to significant variation in hardness along the radial direction. The hardness was considerably higher near the edges of the samples as compared to those

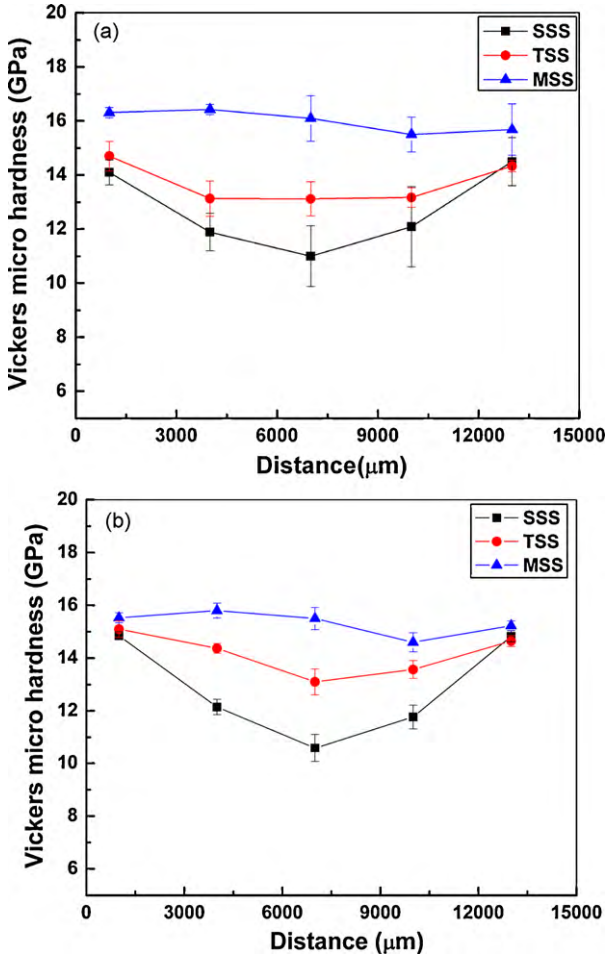

Fig. 6. Variation of Vickers microhardness with radial distance measured from one edge of the sample to the other for (a) T3-ZrO_2 and (b) TM2-ZrO_2, SPS processed via the three different heating schedules of SSS, TSS and MSS. The error bars indicate spread of hardness measured at three different axial positions of 0.5, 1.5 and 2.5 mm from the top surface.

measured near the centres. On the contrary, such variation in hardness along the radial direction was considerably suppressed for the samples, sintered via TSS and was nearly non-existent in the case of MSS. A uniform hardness of ~16 GPa was measured for the ZrO_2 samples, sintered via MSS. To the best of the authors' knowledge, such high hardness value for monolithic ZrO_2 nanoceramics (mostly developed via single stage spark plasma sintering) has never been reported earlier.[2,10,17] The hardness values near the edges (close to the die walls) for TM2-SSS/TSS were similar to that of TM2-MSS. However, in contrast to that for TM2-MSS, much lower hardness values were obtained near the sample cores in the case of TSS (13–14 GPa) and especially on sintering via SSS scheme (9–11 GPa). These observations indicate that increasing the number of intermediate holding stages during the heating cycle of SPS processing (as in MSS scheme) leads to more uniformity and improvement in the mechanical properties of the as sintered materials.

Room temperature flexural strength values for the SPS processed T3-ZrO_2 and TM2-ZrO_2 nanoceramics are presented in Table 1. The strengths measured the TM2-ZrO_2 samples varied between 600 and 1350 MPa, depending on the sintering scheme (SSS/TSS/MSS), and were considerably higher than the strengths measured with the corresponding T3-ZrO_2 samples (500–750 MPa). More importantly, for the both types of ZrO_2 samples investigated, sintering via MSS resulted in higher strength as compared to TSS and still higher with respect to normal single stage sintering (SSS). More specifically, for T3-ZrO_2 samples, the strength obtained after MSS were ~1.5 times higher than those obtained after SSS, which was more pronounced (~2.1 times) for the TM2-ZrO_2 samples.

3.4. Tribological properties

In order to realize the advantage of finer and more uniform microstructure development, along with superior mechanical properties of the MSS ZrO_2 nanoceramics in wear resistant applications, a set of fretting wear experiments were conducted on SSSed and MSSed TM2-ZrO_2 nanoceramic samples against three mating materials, viz. Al_2O_3, ZrO_2 and steel under iden-

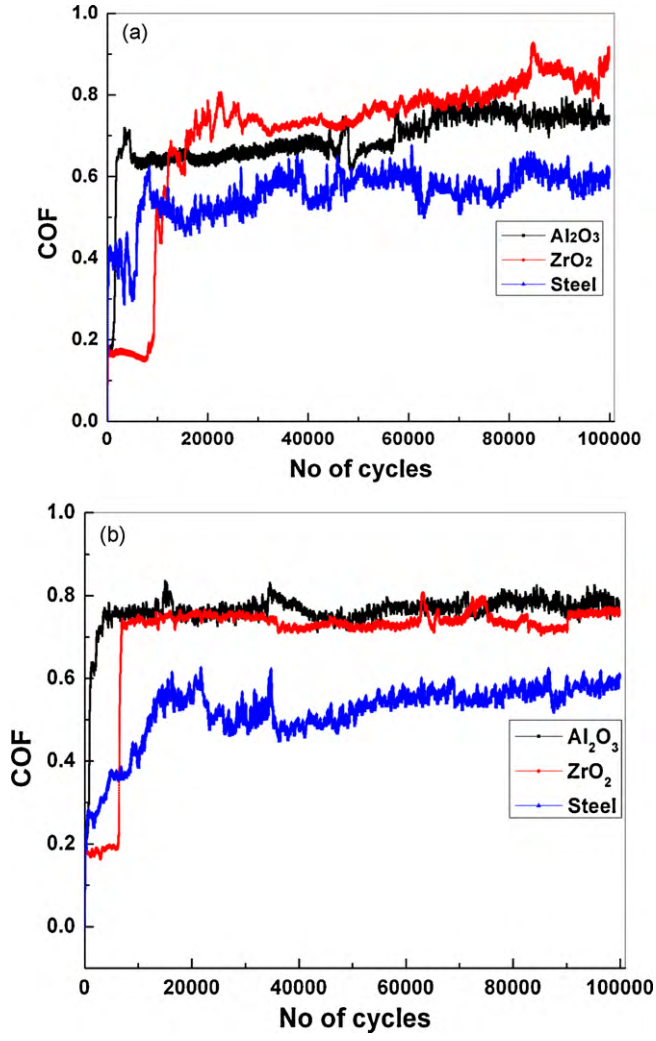

Fig. 7. Plot showing the variation of co-efficient of friction (COF) with fretting duration (as number of cycles) during fretting of against three different counterbodies such as steel, ZrO_2 and Al_2O_3 of TM2-ZrO_2, SPS processed via (a) SSS and (b) MSS. Fretting conditions: 5 N load, 5 Hz frequency, 100,000 cycles and 100 μm stroke length.

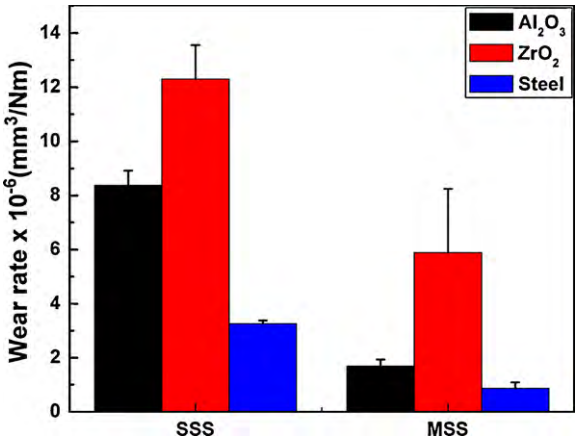

Fig. 8. Wear rates measured for the SPS processed (via SSS and MSS) TM2-ZrO_2 samples after fretting against the three different counterbodies (steel, ZrO_2 and Al_2O_3).

tical operating conditions (load: 5 N; no. of cycles: 100,000; displacement amplitude: 100 μm). The variations of co-efficient of friction (COF) with durations (no. of cycles) during fretting wear against the different counterbodies are presented in Fig. 7. It can be observed that after an initial transient period, the COF settled to a steady state value of ~0.5 for both the ZrO_2 samples during fretting against bearing steel. On fretting against the other two counterbodies, a slight difference in frictional behavior was observed for the ZrO_2 samples processed following the two different processing schemes. While the COF attained a steady state value of ~0.7 after the initial transient period during fretting of the MSSed ZrO_2 samples against both the counterbodies (Al_2O_3 and ZrO_2), the COF recorded with the SSSed ZrO_2 samples presented a slightly increasing trend even after 100,000 fretting cycles, especially against the ZrO_2 counterbody. Hence the COF recorded with the SSSed ZrO_2 eventually reached a value slightly higher than the steady state COFs recorded with the MSSed samples. Furthermore, the COF recorded with the SSSed ZrO_2 samples against all the counterbodies over the entire test durations appeared to be relatively non-uniform, as compared to those recorded with the MSS ZrO_2 samples.

The wear rates of the ZrO_2 nanoceramics (SSSed and MSSed), obtained after fretting against the different counterbodies are presented in Fig. 8. It can be observed that, irrespective of the counterbody material, the wear rate measured with the MSSed ZrO_2 samples (~10^{-7} mm^3/Nm) are nearly an order of magnitude lower than the corresponding wear rates measured with the SSSed ZrO_2 samples (~10^{-6} mm^3/Nm). With respect to the counterbodies, fretting against ZrO_2 self-mated system resulted in maximum wear loss, while against steel resulted in the minimum wear loss for both the ZrO_2 materials under investigation.

4. Discussion

4.1. Correlation between SPS processing scheme, microstructural development and mechanical properties

The dynamic changes in DC pulse current during entire sintering cycle were monitored and plotted in Fig. 9. It can be

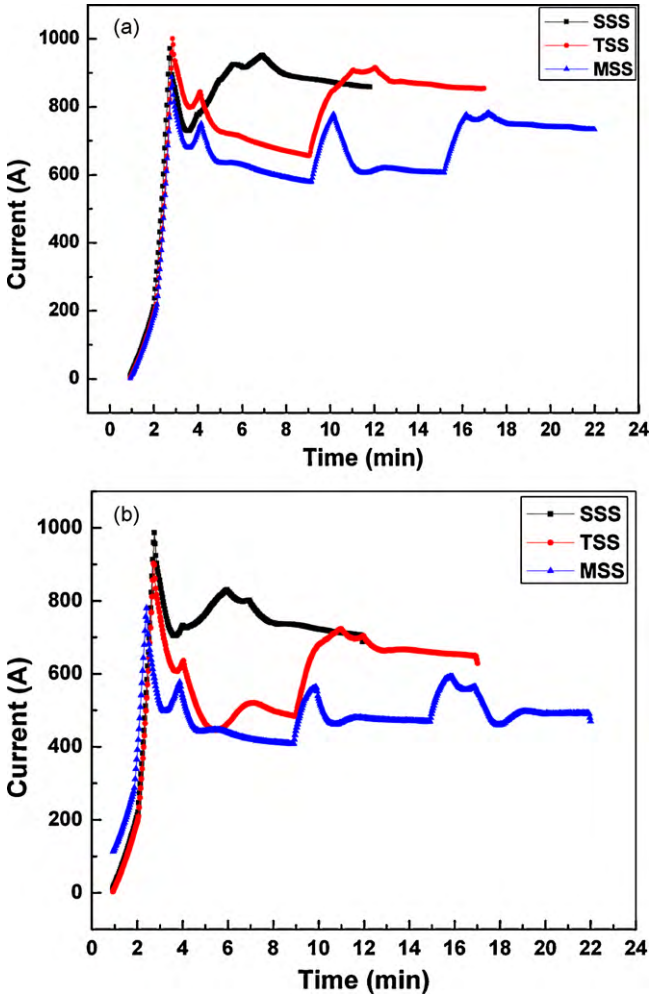

Fig. 9. Plots showing variation of heating current (pulsed DC) with sintering time, recorded for entire heating cycles for three different sintering schedules of SSS, TSS and MSS during SPS processing of (a) T3-ZrO_2 and (b) TM2-ZrO_2.

observed in Fig. 9a and b that current increased at the onset of any holding stage and thereafter decreased to a lower value followed by stabilization during the rest period of holding stage. In the case of MSS, the powder compact experiences three such stabilization of electrical current during the entire heating cycle. We believe that this would cause homogenization of temperature, thereby reducing the temperature gradients across the sample cross-section as well as within the compact in general (between the neck regions). Therefore, neck growth related mass transport can occur in a controlled and more uniform manner for the MSS. Such opportunities of electric current stabilizations during the heating cycle are less in the cases of SSS or TSS. Simulation studies of possible temperature gradients in the compacts during SPS of insulating materials, such as ZrO_2, have indicated that during the sintering stage of normal SSS, the temperature can be much higher near the sample edges (which are in contact with the die) than near the centre.[17,31,32] However, we believe that since the intermediate holding stages of the TSS and MSS schemes provide increased holding duration and opportunities for current stabilization, a more uniform temperature distribution is expected during the final sintering stage. Hence, it is quite obvi-

ous that MSS would result in more uniform densification and concomitantly more uniform microstructural development with respect to SSS or TSS, which agree with the present observations (see Table 1 and Figs. 3–5). The non-uniform temperature distribution and concomitantly the non-uniform densification (see Table 2) in case of SSS are believed to result in the significant variation in hardness observed along the radial directions, which were completely suppressed on processing via MSS scheme (see Fig. 6). Also, the slightly higher sinter densities (see Table 1) and the relatively finer grain sizes (see Figs. 3–5), obtained in the case of MSS, resulted in higher hardness, with respect to SSS.

It is interesting to note that even though the net holding duration (and process time) involved in the MSS scheme is greater than the SSS, relatively finer final grain sizes are obtained with MSS. One of the possible reasons is that in the case of MSS, holding at temperatures around 1000 °C allows more time for the Y^{3+} at segregate to the grain boundaries,[33,34] whereas Y^{3+} segregation is comparatively much suppressed in the case of SSS. It is an established fact that Y^{3+} segregation at ZrO_2 grain boundaries significantly hinders the grain boundary mobility and hence, suppresses the grain growth during the final stage of sintering.[35] We believe that such phenomenon would partly account for the relatively finer grain size development in the case of MSS. This is presently under investigation and will be reported separately. Another possible reason for the relatively reduced grain coarsening in the case of MSS can be correlated with more uniform temperature distribution within the compact, which allows particle coarsening to occur more uniformly during the initial sintering stages. Support for this viewpoint stems from the observations that MSS results not only in finer grain sizes, but also in more uniform final grain size distributions (see Figs. 3 and 4). Additionally, since it is known that electric field suppresses grain coarsening during sintering of ZrO_2,[36] another plausible mechanism influencing the grain refinement in the case of MSS could be related to the more uniformity of electric field and spark discharge that the compact is subjected to due to the intermediate holding stages. On a slightly different note, it can be critically noted that it is the grain sizes near the edges of the samples sintered following SSS scheme that are significantly coarser than the corresponding grain sizes observed with the MSSed samples. The grain sizes near the sample centres are not much different for the SSSed and MSSSed samples. Similar to the arguments concerning the development of relatively higher sinter densities near the edges as compared to the centres in the case of SSS (due to temperature gradient), the grains near the edges and closer (or in contact) to the die are subjected to relatively higher temperatures, which lead to more coarsening. This is suppressed in the case of MSS, due to the temperature distribution being more uniform during the final sintering stages.

More homogeneous densification, along with more uniform development, also contributed to higher flexural strength obtained with the ZrO_2 samples, processed using MSS scheme. Additionally, the relatively finer nanosized grains, obtained in the case of MSS, with respect to SSS, also resulted in improvement of flexural strength. In this respect, Fig. 10a shows that the flexural strength decreased monotonically with increase in average grain sizes for the ZrO_2 samples. Furthermore,

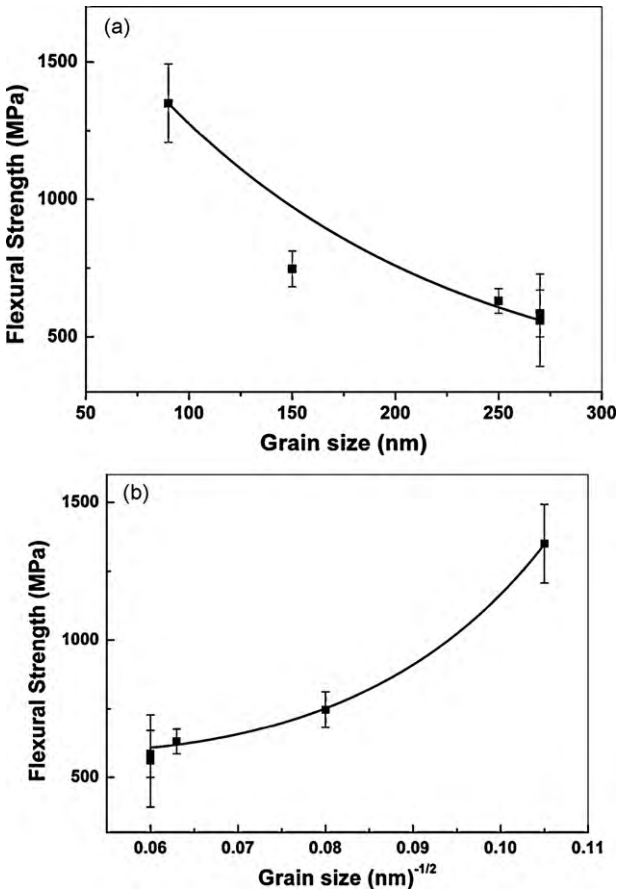

Fig. 10. Variations of flexural strength with (a) mean grain size and (b) inverse of square root of grain size (showing Hall–Petch type of relationship) for all the SPS processed ZrO_2 samples.

a near-linear behavior was obtained on plotting the flexural strengths against the inverse square root of the grain sizes (see Fig. 10b). Such plot indicates that for the SPS processed ZrO_2 samples, a Hall–Petch type relationship can be obtained for flexural strength, as given by the following equation;

$$\sigma = \sigma_0 + kd^{-1/2} \quad (2)$$

where σ is the measured flexural strength, σ_0 is the flexural strength at an infinite grain size, k is the Hall–Petch constant and d is the average grain size. Since the critical crack size in brittle ceramics scales with the larger grain size of the microstructure and considering that the grain size of the investigated ceramics varies in the same order of magnitude (50–400 nm for SSS and 100–150 nm for MSS), the nature of strength limiting critical flaws will be of similar scale. Also, XRD investigation of the fracture surfaces did not reveal the presence of monoclinic zirconia and therefore stress induced tetragonal zirconia phase transformation during fracture can be ruled out in the present case.

4.2. Wear mechanisms and the relationship with mechanical properties

Similar to the mechanical properties, the fretting wear results indicates that the ZrO_2 samples SPS processed following the

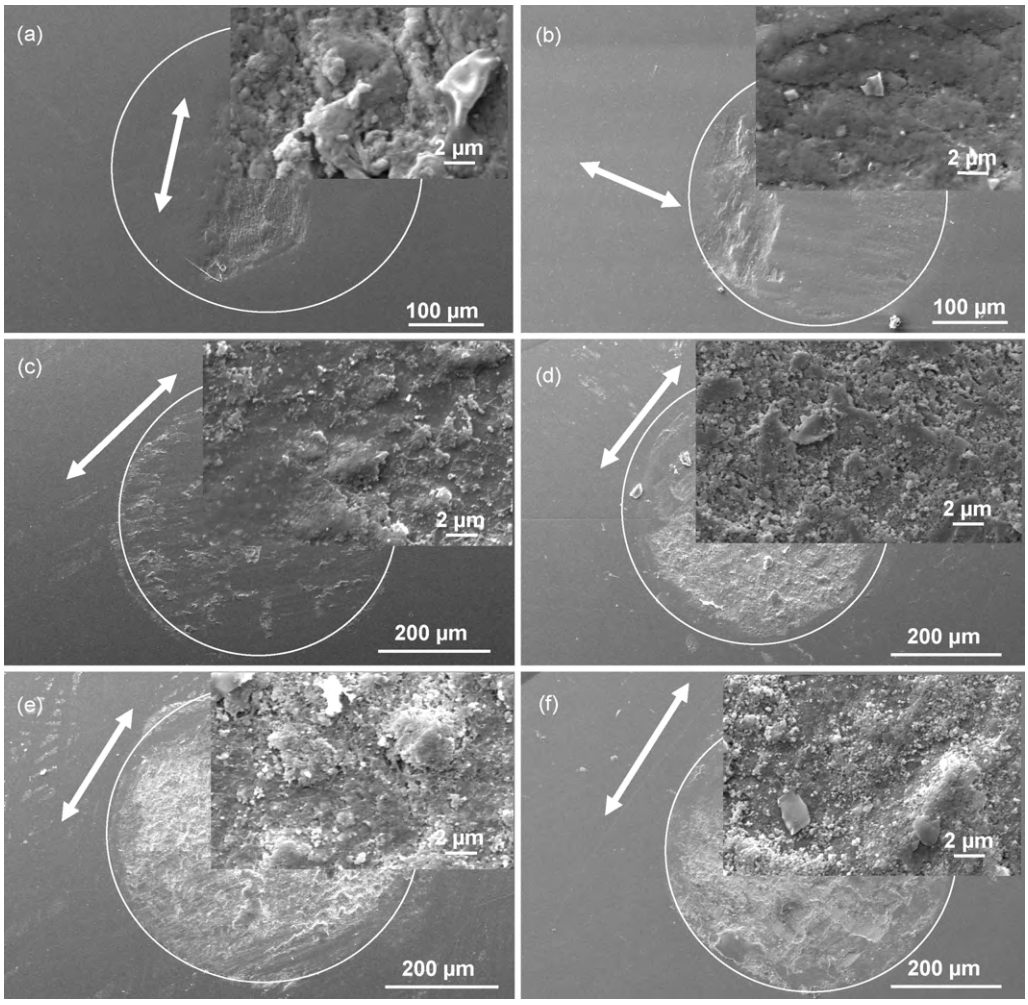

Fig. 11. Low magnification and corresponding higher magnification (as insets) SEM images obtained from the worn surfaces of SPS processed of TM2-ZrO_2, developed via (a, c and e) SSS and (b, d and f) MSS sintering schemes , fretted against (a and b) Al_2O_3; (c and d) steel and (e and f) ZrO_2.

MSS scheme possessed significantly improved wear resistance, with respect to the samples sintered via SSS scheme. This can be attributed broadly to the relatively finer average grain size with unimodal grain size distribution, and higher hardness achieved in the case of MSS.

In order to critically understand the micromechanisms occurring during material removal from the TM2-ZrO_2 surfaces in fretting contact with the various counterbodies, topographical observations of the worn surfaces were made using SEM (see Fig. 11) and the phases present on the worn surfaces were identified with the aid of Raman spectroscopy[37] (see Fig. 12). The abrasive scratches generated mainly due to the abrasive wear of both the types of ZrO_2 nanoceramics can be observed in the SEM images obtained from the worn surfaces fretted against all the counterbodies (see Fig. 11). In this respect, the higher hardness of the MSS sample minimized the damage from abrasive wear and contributed to the improved wear resistance of the MSSed ZrO_2 nanoceramics. Microcracking was observed, especially on the worn surfaces of the SSSed ZrO_2 nanoceramics, with few evidences of brittle fracture induced grain pull-outs. Such mechanism of material removal, along with the formation of ribbon shaped particles, has also been reported earlier for ZrO_2.[38,39] The occurrence of these tribomechanical wear induced material removal appeared to be relatively suppressed for the MSSed ZrO_2 nanoceramics. Raman spectroscopy experiments revealed that in addition to the presence of characteristic t-ZrO_2 bands (located at 149, 255, 318, 464, 640 cm^{-1}), characteristic bands for monoclinic ZrO_2 (located at 181, 337, 472, 560 and 634 cm^{-1}) were also present in the Raman spectra obtained from the worn surfaces of the SSSed ZrO_2 (see Fig. 12a). On the contrary, Raman spectra obtained from the worn surfaces of MSSed ZrO_2 samples did not show the presence of any band corresponding to m-ZrO_2 (see Fig. 12b). Such observations provide strong evidence that fretting wear of SSSed ZrO_2 was accompanied by the phase transformation of tetragonal to monoclinic phase, while such transformation was suppressed for the MSSed ZrO_2 samples. It is very likely that the extensive microcracking observed on the worn surfaces of the SSSed ZrO_2, as opposed to the worn surfaces of the MSSed ZrO_2, could have partly been caused due to the t → m-ZrO_2 phase transformation and the associated strain.[15,40] The relatively finer grain sizes of the MSSed ZrO_2 is believed to be responsible for rendering greater stability to the t-ZrO_2 phase under the fretting wear conditions. In a recent work it has been reported that for monolithic 3Y-

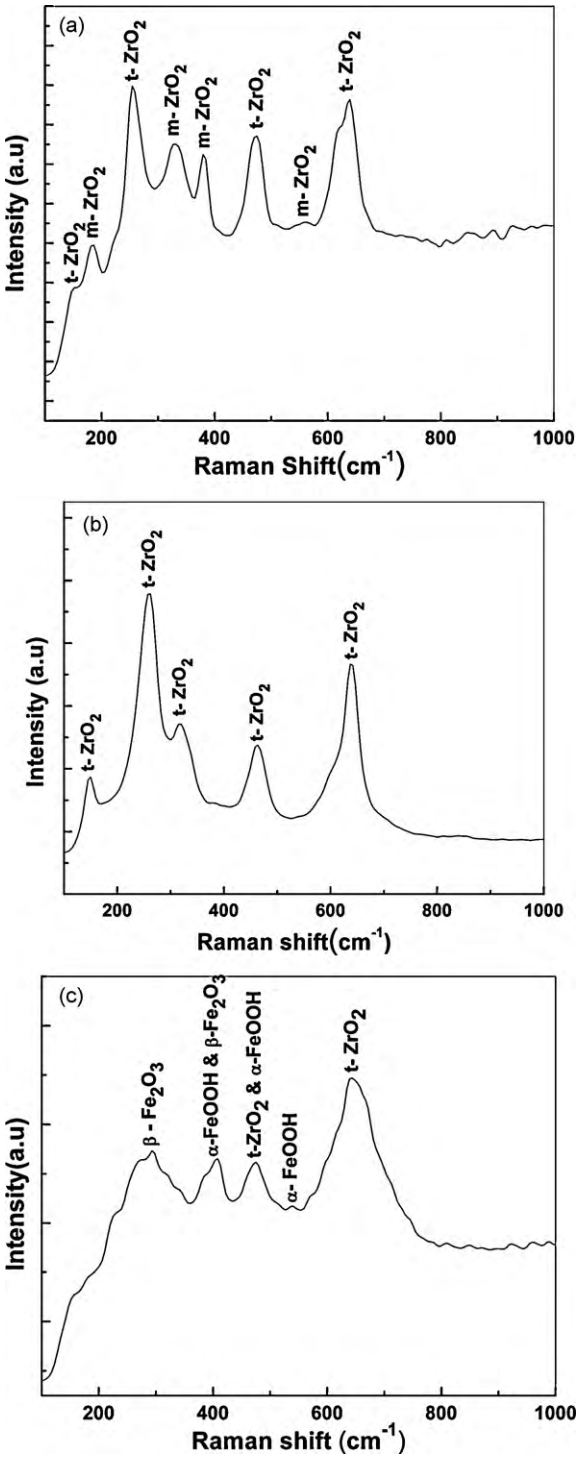

Fig. 12. Raman spectra obtained from the worn surfaces of (a) single stage sintered TM2-ZrO_2 sample after fretting against Al_2O_3 counter body; (b) multi stage sintered TM2-ZrO_2 sample after fretting against Al_2O_3 counter body and (c) multi stage sintered TM2-ZrO_2 sample after fretting against steel counter body.

TZP ceramics t-ZrO_2 phase is stabilized by the ultrafine grain sizes below a critical grain size (D_c) of ~275 nm.[17,28] For the presently investigated TM2-ZrO_2 ceramics, grains with sizes greater than such D_c were formed during SSS. However, all the t-ZrO_2 grains observed in the MSSed sample were less than 150 nm in size (that is below the D_c) (see Figs. 3–5). Hence such phase transformation induced microcracking is believed to be one of the contributing factors towards the lower wear resistance of the SSSed TM2-ZrO_2 samples with respect to the MSSed TM2-ZrO_2 nanoceramics. Such effect of grain size on the wear resistance of monolithic yttria-stabilized tetragonal zirconia polycrystals has also been reported earlier.[40]

SEM images obtained from the worn surfaces of the TM2-ZrO_2 samples fretted against steel show the presence of wear debris and evidences for the formation of tribolayers. The wear debris is observed to be mainly accumulated around the edge of the wear pit. Compositional analysis, via EDX, of the wear debris and tribolayers on the flats revealed the presence of Fe and O. Also, Raman spectroscopy of the worn surface of MSSed TM2-ZrO_2 (fretted against steel) revealed the presence of β-Fe_2O_3 bands (at 298, 414 cm^{-1}) and α-FeOOH bands (at 414, 474 and 550 cm^{-1}), in addition to t-ZrO_2 (see Fig. 12c). These suggest that the tribolayers were formed due to transfer of materials from the steel counterbody. It is likely that the steel ball got oxidized to form Fe_2O_3, which further reacted with atmosphere to form FeOOH under the fretting conditions.[41] We believe that the lower hardness of steel counterbody and formation of protective transfer layer contributed to the lower wear loss against steel with respect to the other ceramic counterbodies (Al_2O_3 and ZrO_2). In this respect, it can also be observed that the transfer layer formed on the MSSed ZrO_2 sample after fretting against steel was continuous and larger in area and hence appeared to be more protective compared to the intermittent layer formed on the worn surface of the SSSed ZrO_2 sample. The relatively higher hardness of the MSSed ZrO_2 sample is likely to have resulted in greater rate of removal of material from the steel counterbody during fretting, which formed the more continuous transfer layer on the MSSed ZrO_2 surface. This is one of the factors responsible for the lower wear rate obtained for MSSed ZrO_2 after fretting against steel, as compared to that obtained for the SSSed ZrO_2. Hence, the present work enabled us to gain an insight into the processing-microstructure development-mechanical/tribological properties of ultrafine grained t-ZrO_2 ceramics, processed via the three different SPS processing schemes. It has been demonstrated that MSS is equally efficient in producing homogeneous densification and more uniform as well as finer microstructural development for both the t-ZrO_2 types studied (T3-ZrO_2 and TM2-ZrO_2). Such microstructure development led to improved mechanical and tribological properties for the ZrO_2 ceramics processed via MSS scheme, with respect to those produced via normal single stage sintering scheme.

5. Conclusions

The present work explored the effects of spark plasma sintering via the innovative two stage sintering (TSS) and multistage sintering (MSS) schemes, as against the commonly used single stage sintering (SSS) scheme, on the microstructural development and concomitantly on the mechanical properties of two types of ZrO_2 samples [commercially available 3 mol% yttria-stabilized ZrO_2 (T3-ZrO_2) and 2:1 mixture of 3Y-ZrO_2 and

0Y-ZrO_2; 2 mol% yttria-stabilized (TM2-ZrO_2)]. Based on the experimental results and analysis, the following conclusions have been reached.

SPS processing at 1250 °C resulted in the development of near theoretical densities for all the ZrO_2 samples. Homogeneous densification along the radial direction (from centre to edges) was observed in the case of MSS, as opposed to SSS. MSS also resulted in the suppression of grain growth relative to SSS, allowing the development of dense ZrO_2 ceramics possessing nanosized grains ∼100–150 nm. Furthermore, much uniform grain size distribution was obtained in the case of MSS.

In case of SSS, a significant variation in hardness was observed along the radial direction, with lower hardness (by ∼5 GPa) near the centre with respect to the regions near the sample edges. Such variation was relatively suppressed in the case of TSS and completely eliminated in the case of MSS, resulting in uniform hardness. It is believed that prevention of the temperature gradient normally associated with SPS processing (via SSS) of insulating ceramics, along with more homogeneous neck growth aided by the intermediate holding stages, resulted in more uniform densification and hence uniform mechanical properties. This is consistent with the density variation and grain size distribution (GSD) throughout the sample.

Overall higher hardness (∼16 GPa) and flexural strengths (∼1.4 GPa for TM2-ZrO_2) were obtained with MSS, with respect to SSS. These were attributed to the relatively finer grain size and more homogeneous microstructure development achieved on spark plasma sintering via the innovative MSS scheme. A Hall–Petch type relationship was observed between flexural strength and grain size. Also, the flexural strengths of the TM2-ZrO_2 samples were higher by nearly a factor of ∼2 with respect to the T3-ZrO_2 samples, processed following the same scheme.

Fretting wear results showed that the ZrO_2 samples processed following the MSS scheme possessed significantly improved wear resistance, with respect to the samples sintered via SSS scheme. This was attributed broadly to the relatively finer average grain size with unimodal grain size distribution and higher hardness achieved in the case of MSS.

Finer grain sizes obtained in the case of MSS, stabilized the t-ZrO_2 phase and suppressed the stress induced transformation to m-ZrO_2 during fretting against Al_2O_3 and ZrO_2 counterbody. This resulted in minimization of microcracking induced fretting wear for the samples processed via MSS, as compared to those processed via SSS. During fretting against steel counterbody, the higher hardness obtained in the case of MSS led to the formation of a more protective transfer layer on the ZrO_2 surface due to higher rate of material removal from the steel counterbody. Hence lower wear rate was observed with respect to ZrO_2 processed via SSS.

Acknowledgements

The author would like to thank Late Prof. R. Balasubramaniam for allowing the use of scanning electron microscope facility. I would also like to express sincere gratitude to the research grant provided by Department of Science and Technology (DST), and the work was financially supported from the Indian Institute of Technology, Kanpur, India.

References

1. Orru R, Licheri R, Locci AM, Cincotti A, Cao G. Consolidation/synthesis of materials by electric current activated/assisted sintering. *Mater Sci Eng R* 2009;**63**:127–287.
2. Mukhopadhyay A, Basu B. Consolidation-microstructure-property relationships in bulk nanoceramics and ceramic nanocomposites. *Int Mater Rev* 2007;**52**:257–88.
3. Gao L, Shen Z, Miyamoto H, Nygren M. Superfast densification of oxide/oxide ceramic composites. *J Am Ceram Soc* 1999;**82**:1061–3.
4. Chen DJ, Mayo MJ. Rapid rate of heating of nanocrystalline ZrO_2–3 mol% Y_2O_3. *J Am Ceram Soc* 1996;**79**:906–12.
5. Chen DJ, Mayo MJ. Densification and growth of ultrafine 3 mol% Y_2O_3-ZrO_2 ceramics. *Nanostruct Mater* 1993;**2**:469–78.
6. Guo SQ, Nishimura T, Kagawa Y, Yang JM. Spark plasma sintering of zirconium diborides. *J Am Ceram Soc* 2008;**91**:2848–55.
7. Li W, Gao L. Fabrication of Hap-ZrO_2 (3Y) nano-composite by SPS. *Biomaterials* 2003;**24**:937–40.
8. Mei B, Miyamoto Y. Preparation of Ti–Al intermetallic compounds by spark plasma sintering. *Metall Mater Trans A* 2001;**32**:843–7.
9. Watari F, Yokoyama A, Omori M, Hirai T, Kondo H, Uo M, Kawasaki T. Biocompatibility of materials and development to functionally graded implant for bio-medical application. *Compos Sci Technol* 2004;**64**:893–908.
10. Li W, Gao L. Rapid sintering of nanocrystalline ZrO_2 (3Y) by spark plasma sintering. *J Eur Ceram Soc* 2000;**20**:2441–5.
11. Angerer P, Yu LG, Khor KA, Korb G, Zalite I, Spark-plasma-sintering. (SPS) of nanostructured titanium carbonitride powders. *J Eur Ceram Soc* 2005;**25**:1919–27.
12. Anselmi-Tamburini U, Gennari S, Garay JE, Munir ZA. Fundamental investigations on the spark plasma sintering/synthesis process. II. Modelling of current and temperature distributions. *Mater Sci Eng A* 2005;**394**:139–48.
13. Tiwari D, Basu B, Biswas K. Simulation of thermal and electric field evolution during spark plasma sintering. *Ceram Int* 2009;**35**:699–708.
14. Vanmeensel K, Laptev A, Hennicke J, Vleugels J, Van Der Biest O. Modelling of the temperature distribution during field assisted sintering. *Acta Mater* 2005;**53**:4379–88.
15. Basu B. Toughening of yttria-stabilised tetragonal zirconia ceramics. *Int Mater Rev* 2005;**50**:239–55.
16. Bernard-Granger G, Guizard C. Spark plasma sintering of a commercially available granulated zirconia powder. I. Sintering path and hypotheses about the mechanism(s) controlling densification. *Acta Mater* 2007;**55**:3493–504.
17. Basu B, Lee JH, Kim DY. Development of nanocrystalline wear-resistant Y-TZP ceramics. *J Am Ceram Soc* 2004;**87**:1771–4.
18. Nygren M, Shen Z. On the preparation of bio-, nano- and structural ceramics and composites by spark plasma sintering. *Solid State Sci* 2003;**5**:125–31.
19. Bernard-Granger G, Monchalin GN, Guizard C. Comparisons of grain size-density trajectory during spark plasma sintering and hot-pressing of zirconia. *Mater Lett* 2008;**62**:4555–8.
20. Juy A, Anglada M. Strength and grinding residual stresses of Y-TZP with duplex microstructures. *Eng Fail Anal* 2009;**16**:2586–97.
21. Zhou Y, Ge QL, Lei TC. Microstructure and mechanical properties of ZrO_2–2 mol% Y_2O_3 ceramics. *Ceram Int* 1990;**16**:349–54.
22. Yoshimura M, Ohji T, Sando M, Nihara K. Rapid rate sintering of nanograined ZrO_2-based composites using pulse electric current sintering method. *J Mater Sci Lett* 1988;**17**:1389–91.
23. Denry I, Kelly JR. State of the art of zirconia for dental applications. *Dent Mater* 2008;**24**:299–307.
24. Maca K, Pouchly V, Zalud P. Two-step sintering of oxide ceramics with various crystal structures. *J Eur Ceram Soc* 2010;**30**:583–9.
25. Wang CJ, Huang CY, Wu YC. Two-step sintering of fine alumina–zirconia ceramics. *Ceram Int* 2009;**35**:1467–72.

26. Chen IW, Wang XH. Sintering dense nanocrystalline ceramics without final-stage grain growth. *Nature* 2000;**404**:168–71.
27. Tartaj J, Tartaj P. Two-stage sintering of nanosize pure zirconia. *J Am Ceram Soc* 2009;**92**:103–6.
28. Mazaheri M, Simchi A, Golestani-Fard F. Densification and grain growth of nanocrystalline 3Y-TZP during two-step sintering. *J Eur Ceram Soc* 2008;**28**:2933–9.
29. Maca K, Pouchly V, Shen Z. Two-step sintering, spark plasma sintering of Al_2O_3 ZrO_2 and $SrTiO_3$ ceramics. *Integ Ferroelectr* 2008;**99**:114–24.
30. Reddy KM, Kumar N, Basu B. Innovative multi-stage spark plasma sintering to obtain strong and tough ultrafine-grained ceramics. *Scripta Mater* 2010;**62**:435–8.
31. Vanmeensel K, Laptev A, Van Der Biest O, Vleugels J. Field assisted sintering of electro-conductive ZrO_2-based composites. *J Eur Ceram Soc* 2007;**27**:979–85.
32. Rathel J, Herrmann M, Beckert W. Temperature distribution for electrically conductive and non-conductive materials during field assisted sintering (FAST). *J Eur Ceram Soc* 2009;**29**:1419–25.
33. Theunissen GSAM, Winnubst AJA, Burggraaf AJ. Surface and grain boundary analysis of doped zirconia ceramics studied by AES and XPS. *J Mater Sci* 1992;**27**:5057–66.
34. Reddy KM, Kumar N, Basu B. Inhibition of grain growth during the final stage of multi-stage spark plasma sintering of oxide ceramics. *Scripta Mater* 2010;**63**:585–8.
35. Li W, Gao L. Compacting and sintering behavior of nano ZrO_2 powders. *Scripta Mater* 2001;**44**:2269–72.
36. Yang D, Conrad H. Enhanced sintering rate of zirconia (3Y-TZP) by application of a small AC electric field. *Scripta Mater* 2010;**63**: 328–31.
37. Li M, Feng Z, Xiong G, Ying P, Xin Q, Li C. Phase transformation in the surface region of zirconia detected by UV Raman spectroscopy. *J Phys Chem B* 2001;**105**:8107–11.
38. Bhusan B. *Principles and applications of tribology*. Wiley Inter. Sci. Pub.; 1999. p. 479–570.
39. He Y, Winnubst L, Burggraaf AJ, Verweij H, Van der Varst PGTh, De With B. Grain-size dependence of sliding wear in tetragonal zirconia polycrystals. *J Am Ceram Soc* 1996;**79**:3090–6.
40. Basu B, Vleugels J, Van Der Biest O. Microstructure-toughness-wear relationship of tetragonal zirconia ceramics. *J Eur Ceram Soc* 2004;**24**:2031–40.
41. Thibeau RJ, Brown CW, Heidersbach RH. Raman spectra of possible corrosion products of iron. *Appl Spectrosc* 1978;**32**:532–5.